Decomposition-based recovery of absorbers in turbid media

S. D. Campbell, I. L. Goodin, S. D. Grobe, Q. Su, and R. Grobe
Intense Laser Physics Theory Unit and Department of Physics, Illinois State University, Normal, Illinois 61790-4560, USA
(Received 12 July 2007; published 6 December 2007)

We suggest that the concept of the point-spread function traditionally used to predict the blurred image pattern of various light sources embedded inside turbid media can be generalized under certain conditions to predict also the presence and location of spatially localized absorbing inhomogeneities based on shadow point-spread functions associated with each localized absorber in the medium. The combined image obtained from several absorbers can then be decomposed approximately into the arithmetic sums of these individual shadow point-spread functions with suitable weights that can be obtained from multiple-regression analysis. This technique permits the reconstruction of the location of absorbers.

DOI: 10.1103/PhysRevA.76.063802 PACS number(s): 42.25.Dd, 42.30.Lr

I. INTRODUCTION

The interaction of electromagnetic radiation with highly scattering materials [1,2] is of interest in a wide variety of research areas including astrophysics, nuclear physics, and medicine. In medicine the goal is to use the scattered light to obtain some information about the optical properties inside the medium [3]. The Boltzmann equation is often used to model how a laser field propagates through the medium. It requires information about the scattering phase function and the spatially dependent absorption and scattering coefficients. As this equation is linear in irradiance, formal solutions to the forward problem can be given in terms of Green's functions. Among the popular models to approximate the forward solution is the diffusion kernel, which can be given analytically for simplified geometries [4]. For inverse problems [5], the space-dependent scattering coefficient is typically linearized in the corresponding propagation kernel [6–8]. Based on this linearization, inverse techniques can be applied to find the scattering coefficient as a function of the properties of the scattered light [9].

In this paper we will explore the question under which conditions the solution to the nonlinear propagation kernel of the forward problem can be decomposed into a finite set of linear superpositions of special forward solutions that are associated with a set of simpler spatial structures such as localized reflectors or absorbers that are embedded in the medium. For example, the measured scattered light (called the image here) from several light sources inside the medium is identical to the arithmetic sum of the individual images associated with each light source [10–12]. Due to the nonlinear dependence of the image on the scattering and absorption coefficients, it is not clear, however, if a similar decomposition can be accomplished for those objects inside the medium that modify the light. If such decomposition is possible, then the task of reconstructing complicated objects can become possible based on the knowledge of a set of basis states. These necessary basis states associated with simpler inhomogeneities can be obtained by direct measurements or by computations.

The basic idea to deconvolute a nonlinear integration kernel using a linear superposition of given basis states with unknown weights is not new. For example, in observational astronomy the images of galaxies were decomposed into linear superpositions of localized functions with different shapes, called shapelets [13] in order to classify the types of galaxies. Shapelets are also used as a method to decompress images and in applications in optical coherence tomography [14].

The paper is organized as follows: In Sec. II, we will use a simple forward model to show under which conditions the brightness pattern associated with several absorbers can be linearly decomposed into the sum of patterns associated with only a single absorber, each. In Sec. III, we will examine the completeness relationship experimentally by detecting the brightness pattern scattered off a tank filled with a milk-water solution and various absorbers. We will conclude with an outlook on new challenges for future work.

II. MODEL AND RESULTS

A. Analytical model: A two-absorber system

The interaction of an electromagnetic field with a turbid medium is usually described by the radiative transfer (Boltzmann) equation [1,2]. for which the light distribution is modeled by the position $\mathbf{r}$- and velocity $\mathbf{\Omega}$-dependent irradiance $I(\mathbf{r},\mathbf{\Omega})$. The physical origin of the light is modeled by a source term that is added to this equation. As a consequence of this formalism, the solutions are linear in the source terms, in other words, the resulting solution for two light sources is identical to the arithmetic sum of the solutions associated with only one source, $I_{1\&2}(\mathbf{r},\mathbf{\Omega})=I_1(\mathbf{r},\mathbf{\Omega})+I_2(\mathbf{r},\mathbf{\Omega})$.

This principle of linearity with respect to the sources, however, does not automatically guarantee that a unique decomposition of the image into the underlying images associated with each source term is always possible. Often, only a partial or averaged information of $I(\mathbf{r},\mathbf{\Omega})$ can be obtained experimentally—e.g., a position-dependent brightness $B(\mathbf{r}) \equiv \int\int d\mathbf{\Omega}\, I(\mathbf{r},\mathbf{\Omega})$, where the spatial region of $\mathbf{r}$ is finite and typically outside the medium. In this case, $B(\mathbf{r})$ could provide insufficient information for a unique decomposition. For example, two highly directional light sources emitting along the same optical axis lead in vacuum to nearly identical brightness patterns independently of their distance from the detector, $B_1(\mathbf{r}) \approx B_2(\mathbf{r})$. A unique decomposition of the two-

source brightness signal into $B_1(\mathbf{r})$ and $B_2(\mathbf{r})$ is not possible. If, however, the sources are embedded in a turbid medium, the brightness patterns will be different permitting a unique decomposition into the underlying single-source patterns.

The central question we try to address in this work is whether a similar decomposition-based imaging approach can be generalized to identify also light distribution modifying objects such as spatially localized absorbers, reflectors, or combinations of both. As the scattering and absorption coefficients $\mu_s(\mathbf{r})$ and $\mu_a(\mathbf{r})$ enter the Boltzmann equation as multiplicative factors to $I(\mathbf{r},\mathbf{\Omega})$, the resulting forward solution is nonlinear in these optical coefficients. As a result, one might (incorrectly) expect that the resulting brightness patterns cannot be used to reconstruct the location of the objects.

To answer this fundamental question, let us examine the simplest possible model system. We assume a light field with brightness along the transverse direction given by $B(x=0,\ y,\ z=1)$ enters from the right side of a turbid medium at $z=1$. The scattering medium is located between $0<z<1$ and is infinitely extended along the other two directions x and y. Let us assume we place two perfect absorbers at position $(0,\ 0,\ z=0)$ and a second one at $(0,\ 0,\ z=1)$. The transmitted light is detected at the left side of the medium at $z=0$, directly behind the location of the first absorber. In vacuum, each of the absorbers would create an identical shadow pattern. If the medium is turbid, however, we will show below, that—similarly to the linearity of the brightness patterns for the light sources—also the resulting shadow pattern [15] of both absorbers can be related to the two individual shadow patterns associated with each single absorber.

The resulting relationship for absorbers is only slightly more complicated than for the light sources. Let us first define the shadow functions

$$S_{ij}(y) \equiv B_{00}(x=0,y,z=0) - B_{ij}(x=0,y,z=0), \quad (2.1)$$

where the subscripts $i,j=0,1$ reflect the presence (1) or absence (0) of an absorber at locations z_1 and z_2. For example, $B_{01}(y)$ denotes the brightness pattern caused by no absorber at location z_1 and one absorber at location z_2. The shadow function $S_{ij}(y)$ is therefore a direct measure of the spatial distribution of the blocked light. If both absorbers were placed not behind each other (on the z axis), but at different transverse locations y such that the resulting shadow patterns $S_{10}(y)$ and $S_{01}(y)$ would not spatially overlap, we would expect full linearity to hold: $S_{11}(y)=S_{10}(y)+S_{01}(y)$. The interesting question now is if a generalized principle of linearity can be applied if the absorber closer to the light source (at $z=1$) can block the incoming light for the other absorber (at $z=0$), resulting in a spatially overlapping shadow pattern. Is it then possible to find two shadow strength parameters λ_1 and λ_2, such that we have

$$S_{11}(y) = \lambda_1 S_{10}(y) + \lambda_2 S_{01}(y)? \quad (2.2)$$

Or is the resulting shadow pattern of two absorbers $S_{11}(y)$ functionally so different from $S_{10}(y)$ and $S_{01}(y)$ such that other functions are required for a complete decomposition?

In order to examine this question theoretically, one would have to solve the Boltzmann equations for configurations with zero, one, and two absorbers. In order to obtain a faster and partially analytical answer, we have to model the formation of the shadow. Let us neglect the direction of the light and assume that the brightness of the detected light is simply related to the brightness of the light before it enters the medium at $z=1$ independently of the propagation direction, denoted by $L(y,z=1)$. This brightness function can then be mapped onto the function $L(y,z=0)$ [identical to $B(y)$] by the consecutive action of the scattering and absorption operators M_s and M_a. The two operators are defined in this model as

$$M_s L(y) \equiv \int dy' h_s(y-y') L(y), \quad (2.3a)$$

$$M_a L(y) \equiv h_a(y) L(y). \quad (2.3b)$$

In the numerical example below, we use $h_s(y) \equiv (2\pi m_s^2)^{(-1/2)} \exp[-y^2/(2m_s^2)]$ and $ha(y) \equiv \{1-ma \exp[-(y-2)2/(2Da2)]\}$. The parameter m_s in the kernel for the convolution in Eq. (2.3a) is related to the usual scattering coefficient μ_s of the Boltzmann equation, but its units are that of length. It is proportional to the transverse spatial region into which a narrow incoming beam is scattered into. The limiting case of vacuum would be modeled by $m_s=0$, making M_s the identity operator. The parameter D_a reflects the (transverse) spatial extension of the absorber that we place arbitrarily at location $y=2$, and m_a is a measure of the opacity due to absorption. Note that the action of M_a amounts to "burning" a Gaussian-shaped hole (shadow) in the brightness pattern $L(y)$.

Depending on the presence and location of the absorbers, we can now obtain three different shadow functions

$$S_{10}(y) \equiv [M_s - M_a M_s] L(y), \quad (2.4a)$$

$$S_{01}(y) \equiv [M_s - M_s M_a] L(y), \quad (2.4b)$$

$$S_{11}(y) \equiv [M_s - M_a M_s M_a] L(y). \quad (2.4c)$$

Using these special model solutions, we can now return to Eq. (2.2) and address the question of completeness, in other words, can the two-absorber shadow $S_{11}(y)$ be expressed as a linear combination of the two single-absorber shadows $S_{10}(y)$ and $S_{01}(y)$?

In Fig. 1(a) we illustrate an example for the two shadow functions $S_{10}(y)$ and $S_{01}(y)$ for $m_s=0.3$, $D_a=0.1$, and $m_a=1.0$. We also include as the dashed line the input brightness function $L(y)=\exp[-(y-2)^2/(2\sigma^2)]$ where σ is related to the transverse spatial width of the incoming Gaussian light field.

One could (incorrectly) expect that the redistribution of light due to m_s would narrow the shadow, as light can scatter into the darker regions and effectively fill up the shadow with light. The graphs, however, show that $S_{01}(y)$ is much wider compared to $S_{10}(y)$, suggesting that a shadow actually *widens* due to the scattering. This widening is a consequence of the conservation of energy. In order to fill up a shadow region, the photons have to leave another region, which becomes darker as a result of this process.

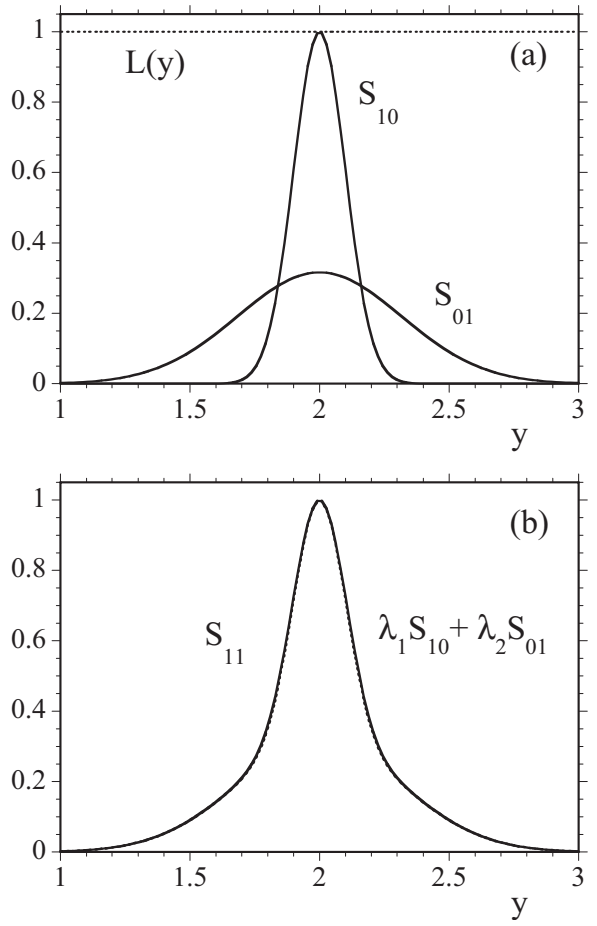

FIG. 1. (a) The shadow functions $S_{10}(y)$ and $S_{01}(y)$, for $m_s=0.3$, $m_a=1$, and $D_a=0.1$ together with the brightness function of the incoming light, $L(y)=1$ (dashed line) corresponding to $\sigma=\infty$. (b) The shadow pattern obtained from two absorbers $S_{11}(y)$ together with a best-fit superposition of $S_{10}(y)$ and $S_{01}(y)$ shown by the dashed line.

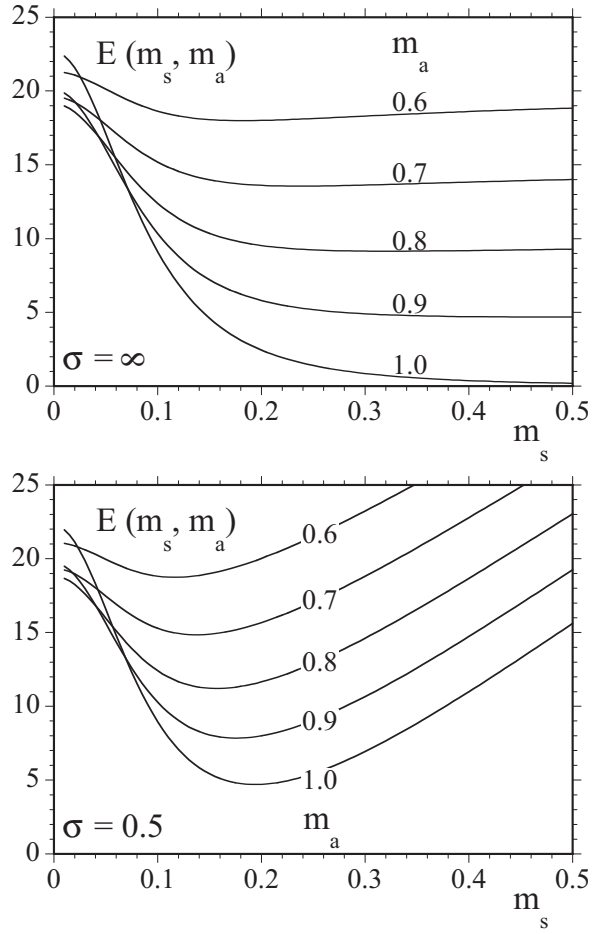

FIG. 2. The error $E(m_s,m_a)$ defined in Eq. (2.6) as a function of m_s for five strengths of the absorber m_a, $D_a=0.1$, and the incoming beam width $\sigma=\infty$ (top) and $\sigma=0.5$ (bottom).

In Fig. 1(b), we compare the two-absorber shadow pattern $S_{11}(y)$ with a superposition of $S_{01}(y)$ and $S_{01}(y)$ shown by the dashed line. The agreement is superb. Here we just chose $\lambda_1=1-S_{01}(y=2)$ and $\lambda_2=S_{11}(y=2)$ as expansion coefficients. In this example it turns out that $\lambda_1=0.683\,90$ and $\lambda_2=0.997\,30$. This particular choice matches $S_{11}(y)$ and $\lambda_1 S_{10}(y)+\lambda_2 S_{01}(y)$ perfectly for $y=2$. This follows directly from the fact that $B_{10}(y)$ and $B_{11}(y)$ vanish at $y=2$ due to the leftmost action of the operator M_a associated with the perfect absorbers at $y=0$. In the experimental section where we analyze more absorbers we will use a multiple-regression technique to find the best possible superposition.

We see that despite the significant spatial overlap of $S_{10}(y)$ and $S_{01}(y)$, the superposition of the two states seems to describe $S_{11}(y)$ quite accurately. We note that even though both absorbers are fully present to determine $S_{11}(y)$, the effective weight for the state $S_{10}(y)$ given by λ_1 is much less than unity. This is related to the blockage of light associated with the second absorber at $z=1$. In order to create effectively a shadow, an absorber would require a sufficient amount of light.

Let us now examine more quantitatively under which conditions of m_s, m_a, D_a, and σ the states $S_{10}(y)$ and $S_{01}(y)$ can form a complete basis for $S_{11}(y)$. A direct measure of the degree of completeness could be the difference between $S_{11}(y)$ and the best-fit superposition of $S_{10}(y)$ and $S_{01}(y)$:

$$\Delta(y) \equiv S_{11}(y) - \{[1 - S_{01}(2)]S_{10}(y) + S_{11}(2)S_{01}(y)\}, \tag{2.5}$$

which due to the particular choice of weights λ_1 and λ_2 fulfills automatically $\Delta(y=2)=0$. In order to have a single number as a measure for completeness, one could define $E(m_s,m_a)$ as the relative error. In order to have a single parameter, the ratio of areas of $\Delta(y)$ and the shadow $S_{11}(y)$ would lead to

$$E(m_s,m_a) \equiv \int dy\, \Delta(y) / \int dy\, S_{11}(y). \tag{2.6}$$

This parameter is zero if the two basis states are complete and the state $S_{11}(y)$ can be expressed as a superposition.

In the top of Fig. 2, we graph this error as a measure of the degree of completeness as a function of the scattering strength m_s for several absorbers for an incoming field of

width $\sigma=\infty$. For the strongest absorber ($m_a=1.0$) the error decreases with increasing scattering strength. For not so strong absorbers ($m_a<0.6$) the method seems to work not so well as the error stays above 18%.

In the vacuum limit ($m_s=0$) the difference function reduces to $\Delta(y)=h_a(y)[1-h_a(y)]L(y)$. It turns out that the maximum value of $h_a(y)[1-h_a(y)]$ for any function $h_a(y)$ ranging from 0 to 1 is given by 1/4, leading to an upper estimate for $\Delta(y)$. In order to maximize the completeness one should use an absorber function that fulfills $h_a(y)^2=h_a(y)$, requiring $h_a(y)$ to be the product of two unit-step functions $h_a(y)=1-\Theta(y-2+D_a/2)\Theta(2+D_a/2-y)$, where $\Theta(y)\equiv(1+|y|/y)/2$.

In order to check the universality of our findings, we graph in the bottom of Fig. 2 the error for an incoming field with a finite transverse width $\sigma=0.5$. In contrast to the broad illumination, the errors decrease only for $0<m_s<0.2$ and then rise as we increase the scattering, suggesting that the technique might work better for a relatively broader input light.

If the incoming beam is narrower than the absorber, $\sigma<D_a$, then the second absorber at $z=1$ blocks out the entire light, leading to a vanishing $S_{01}(y)$ and $S_{11}(y)$, whereas the light could spread first before the absorber at $z=0$ would burn a hole into the widened distribution, leading to a nonvanishing $S_{10}(y)$ for $|y-2|>D_a$.

In summary, we have shown that even in regimes of spatially overlapping shadow regions, the shadow created by two absorbers can be decomposed into the underlying single-absorber shadows. These two states form a complete (nonorthogonal) basis for wide incoming beams and highly scattering systems.

B. Numerical results for the four-absorber system

Let us now generalize the obtained analytical results to a slightly more complicated system of (at most) four rods that are placed along the z axis at locations $z_1=0$, $z_2=1/3$, $z_3=2/3$, and $z_4=1$. The four calibration shadow patterns are denoted by $S_{1000}(y)$, $S_{0100}(y)$, $S_{0010}(y)$, and $S_{0001}(y)$, where we have generalized the notation introduced above. For example, the shadow function $S_{1010}(y)$ is obtained by two absorbers at locations z_1 and z_3 and its spatial form is obtained by the consecutive operation of the scattering and absorption operators, $S_{1010}(y)=[M_sM_sM_s-M_aM_sM_sM_aM_s]L(y)$.

For short we denote the four "basis" states by $V_n(y)$, with $n=1,4$. A typical question would be whether the two-absorber shadow function $S_{1010}(y)$ can be expressed as a linear superposition of the (nonorthogonal) calibration states $S_{1000}(y)$ and $S_{0010}(y)$ only or whether the space spanned only by these two vectors is incomplete to represent $S_{1010}(y)$ and other calibration states such as $S_{1000}(y)$ and $S_{0001}(y)$ or even other functions are required as well. The decomposition was done by using the standard χ^2 linear least-squares fitting approach [16],

$$\chi^2\{\lambda_n\}\equiv\int dy[S_{ijkl}(y)-\sum_{n=1}^{4}\lambda_nV_n(y)]^2/w(y)^2. \quad (2.7)$$

The arbitrary function $w(y)$ can be used to give certain spatial regions in y more weight. For simplicity, we chose

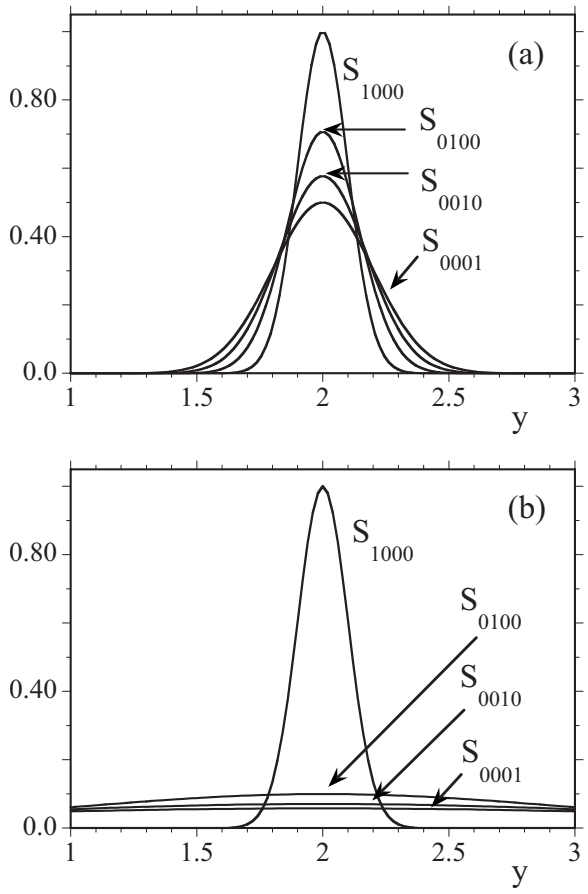

FIG. 3. The four shadow functions $S_{1000}(y)$, $S_{0100}(y)$, $S_{0010}(y)$, and $S_{0001}(y)$ for absorption strength $m_a=1$, absorber diameter $D_a=0.1$, and incoming light width $\sigma=\infty$. The corresponding weight factors of these four modes are displayed in Table I(a) and Table I(b) for 11 arrangements of absorbers. (a) Scattering strength $m_s=0.1$ and (b) scattering strength $m_s=1.0$.

$w(y)=1$. The resulting four linear equations for the weights λ_n can be obtained from the four conditions $\partial\chi^2/\partial\lambda_n=0$. The four weights λ_n are obtained by a simple matrix inversion.

In Figs. 3(a) and 3(b), we graph the four shadow functions for a weaker ($m_s=0.1$) and stronger ($m_s=1$) scattering medium. For simplicity, we used a constant incoming light front $L(y)=1$. For small m_s, the light cannot redistribute itself behind each absorber and the four shadow functions are similar to each other. The shadows for $m_s=1$, however, show a significant spread. The larger the degree of scattering m_s, the more similar are $S_{0010}(y)$ and $S_{0001}(y)$.

A system with a maximum of four absorbers can have 11 different ways to be arranged in addition to the four single-absorber configurations that are used as calibration states. In Table I we have summarize the corresponding weight factors λ_n and in parentheses (0 or 1) we indicate the presence or absence of an absorber. The weights for the weaker scattering medium do not suggest a direct relationship to the actual presence or absence of absorbers. Many modes require negative weights with absolute values larger than unity in order to approximate the image obtained from multiple absorbers. For example, the two-absorber shadow $S_{1100}(y)$ [first row of Table I(a)] requires $\lambda_3=-3.49$ and $\lambda_4=1.496$, even though

TABLE I. The weight factors λ_1, λ_2, λ_3, and λ_4 associated with the shadow calibration states S_{1000}, S_{0100}, S_{0010}, and S_{0001}, respectively, for 11 different absorber combinations. The presence or absence of an absorber is indicated by the number in parentheses. For example, the image decomposed in the last row contains all four absorbers. (a) Theoretical data: scattering strength $m_s=0.1$, absorption strength $m_a=1$, absorber diameter $D_a=0.1$, incoming light width $\sigma=\infty$. Model data for weak scattering of Fig. 3(a). (b) Theoretical data: scattering strength $m_s=1.0$, absorption strength $m_a=1$, absorber diameter $D_a=0.1$, incoming light width $\sigma=\infty$. Model data for large scattering of Fig. 3(b). (c) Experimental data for the four-rod system described in Sec. III. Experimental data of Fig. 5.

λ_1	λ_2	λ_3	λ_4
		(a)	
−0.484 (1)	3.907 (1)	−3.490 (0)	1.496 (0)
−0.021 (1)	1.599 (0)	−0.867 (1)	0.791 (0)
0.206 (1)	1.037 (0)	−1.188 (0)	1.500 (1)
−0.051 (0)	0.200 (1)	1.420 (1)	−0.147 (0)
−0.028 (0)	0.346 (1)	0.274 (0)	0.907 (1)
0.007 (0)	−0.128 (0)	0.462 (1)	1.082 (1)
−0.537 (1)	2.529 (1)	−1.289 (1)	0.999 (0)
−0.464 (1)	2.530 (1)	−2.271 (0)	1.985 (1)
−0.153 (1)	1.407 (0)	−1.298 (1)	1.823 (1)
−0.034 (0)	−0.081 (1)	0.870 (1)	0.944 (1)
−0.455 (1)	1.806 (1)	−1.283 (1)	1.847 (1)
		(b)	
0.901 (1)	1.003 (1)	−0.006 (0)	0.004 (0)
0.930 (1)	0.001 (0)	0.998 (1)	0.001 (0)
0.942 (1)	0.001 (0)	−0.001 (0)	1.001 (1)
0.000 (0)	0.901 (1)	1.000 (1)	0.000 (0)
0.000 (0)	0.930 (1)	0.000 (0)	1.000 (1)
0.000 (0)	0.000 (0)	0.901 (1)	1.000 (1)
0.840 (1)	0.905 (1)	0.992 (1)	0.005 (0)
0.850 (1)	0.933 (1)	−0.007 (0)	1.004 (1)
0.879 (1)	0.002 (0)	0.898 (1)	1.002 (1)
0.000 (0)	0.840 (1)	0.901 (1)	1.000 (1)
0.795 (1)	0.844 (1)	0.893 (1)	1.005 (1)
		(c)	
0.613 (1)	1.113 (1)	−0.081 (0)	0.035 (0)
0.757 (1)	0.182 (0)	0.736 (1)	0.116 (0)
0.790 (1)	0.034 (0)	0.059 (0)	0.949 (1)
−0.040 (0)	0.798 (1)	0.777 (1)	0.121 (0)
−0.019 (0)	0.818 (1)	−0.028 (0)	1.022 (1)
−0.025 (0)	0.131 (0)	0.287 (1)	1.206 (1)
0.571 (1)	0.615 (1)	1.094 (1)	0.011 (0)
0.582 (1)	0.556 (1)	0.427 (0)	0.836 (1)
0.683 (1)	0.046 (0)	0.532 (1)	1.049 (1)
−0.015 (0)	0.458 (1)	0.662 (1)	1.090 (1)
0.480 (1)	0.509 (1)	0.594 (1)	1.155 (1)

there were no absorbers at z_3 and z_4 in this particular case.

The situation improves drastically as we increase the scattering strengths m_s. Modes that are characterized by an absorber that is not present in the multiple-absorber image have nearly vanishing weights. For example, our two-absorber shadow $S_{1100}(y)$ requires $\lambda_3=-0.006$ and $\lambda_4=0.004$, which is a significant improvement over the corresponding weights for $m_s=0.1$. We also note that in the case of S_{1111} the weights increase now monotonically (from left to right). In the limit of very large scattering, $m_s\to\infty$, all weights λ_n approach 1 if the corresponding absorber is present in the superposition.

We have also repeated the simulation for absorbers that were 10 times narrower than in used in Table I(a), with $D_a=0.01$. The results were $\lambda_4=1.00\pm0.002$ for an existing absorber at z_4 and $\lambda_4=0.0\pm0.002$ for one that was absent. This suggests that the narrower the absorbers, the better the method works.

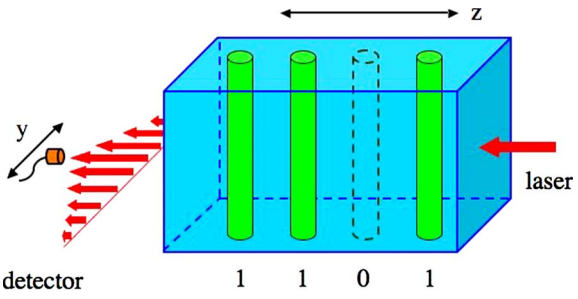

FIG. 4. (Color online) A sketch of the experimental setup with four rods embedded into the tank.

III. EXPERIMENTAL RESULTS

While the system becomes quasilinear and therefore invertible for the theoretical model system discussed above, the technical usefulness of the proposed scheme needs to be examined also experimentally.

The experimental setup is sketched in Fig. 4. We have illuminated a 12-liter glass tank (30.3 cm × 16.3 cm × 25 cm) with a 661-nm diode laser with a power of 80 mW and input beam diameter of about 1 mm. At locations $z=1.8$, 4.1, 6.4, and 8.7 cm from the (inner) exit surface of the tank, we have placed cylinders as absorbers. These plastic rods have a diameter of 0.95 cm and a length of 20.3 cm. As a scattering medium, we used a 2% milk-water mixture with various concentrations. A 3.2-mm-diameter optical fiber bundle connected to a broad-area detector (NewFocus 2031) scanned the scattered light in 221 steps along the y direction, parallel to the exit wall of the tank. The spatial dependence of the brightness was recorded with the LABVIEW software, which also controlled our stepper motors to move the detection fiber.

In a separate work [17–19], we described how one can use measurements of the light distribution inside the medium along the optical axis to determine reliably the scattering and absorption coefficients as well as the anisotropy factor g. For the HeNe laser [17] the empirical formula $\mu_s=\rho\times310\ \mathrm{cm}^{-1}$ approximates the scattering coefficient, where ρ denotes the concentration of 2% milk in the water. For the data presented in Fig. 5 we chose $\rho=100$ ml milk/9.2 l water, suggesting a scattering coefficient of about $\mu_s=3.3\ \mathrm{cm}^{-1}$, leading to an inverse scattering length of about 0.3 cm and with $g=0.93$ to a reduced scattering length of $[\mu_s']^{-1}=4.2$ cm. In other words, rod spacings of either 2.3

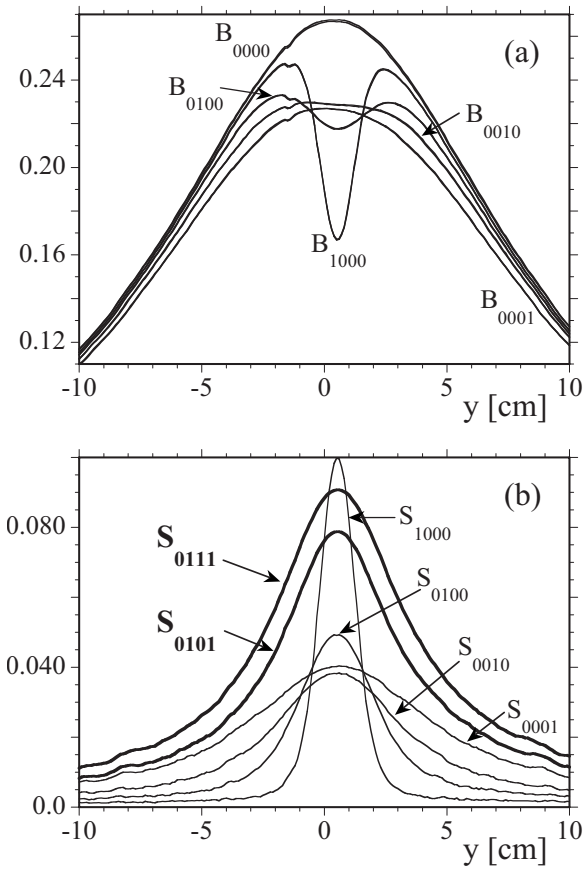

FIG. 5. (a) Experimental brightness functions $B_{0000}(y)$, $B_{1000}(y)$, $B_{0100}(y)$, $B_{0010}(y)$, and $B_{0001}(y)$ for two sets of data. (b) Four experimental shadow calibration functions together with the two- and three-absorber shadows $S_{0101}(y)$ and $S_{0111}(y)$. The corresponding weights for this superposition can be found in Table I(c). The scattering medium was a mixture of 100 ml of 2% milk with 9.2 l of water.

cm, 4.6 cm, or 6.9 cm are much larger than the inverse scattering length in this case.

In order to improve the accuracy, the data were averaged over two independent runs. In Fig. 5(a) we show the four brightness patterns obtained with a single absorber as well as the pattern without any absorber for each of the two runs. The two data sets with the largest hole (B_{1000}) correspond to the arrangement where the absorber is closest to the detector, whereas the shadow effect of the rod closest to the laser source (B_{0001}) is almost completely blurred out due to the scattering.

Similarly as in the discussion on the previous section, we have measured the brightness distribution for 11 different arrangements of the rods. The resulting weights obtained from the averages over two runs are shown in Table I(c). The data clearly suggest that, in principle, a reconstruction of the absorber locations is possible. The only exception is the third weight ($\lambda_3=0.427$) from the shadow pattern for S_{1101}, which is relatively large for a nonexisting absorber. In all other cases the brightness patterns allow an unambiguous recovery of the presence and location of the absorbing rods.

In Fig. 5(b) we show the corresponding four shadow calibration states. In order to illustrate the ability of this technique to resolve the absorbers, we graph in Fig. 5(b) also the two-rod shadow pattern S_{0101} together with the three-rod pattern S_{0111}. These two differ only by the third absorber. The third position is embedded between the fourth and second absorbers, so the question about the ability of the scheme to resolve the presence or absence of this absorber needs to be addressed. This is nontrivial as this region is in the direct shadow of the fourth absorber and its effect on the final brightness distribution might be screened off by the second absorber.

The corresponding shadow patterns shown by the bold graphs are very similar and almost seem to be proportional to each other. If they had the same shape, the decomposition algorithm would not be able to distinguish between the two curves. However, the two curves do not have exactly the same shape and the resulting decomposition predicts with $\lambda_3=0.662$ (tenth row) the presence of the third absorber correctly for S_{0111} and the weight $\lambda_3=-0.028$ (fifth row) suggests correctly the absence of a rod on the third location for S_{0101}. These first experimental results are encouraging as the technique seems to be suitable to distinguish whether there are absorbers at each location.

IV. SUMMARY AND CONCLUSION

In this paper we have suggested theoretically and also experimentally that under suitable conditions the principle of superposition can be extended to apply also to reconstruct the location of spatially localized absorbers. The purpose of this paper is just to provide a proof-of-principle and obviously many more questions need to be addressed to establish any practical feasibility of this technique for imaging in turbid media.

The present study used a well-defined fixed grid of possible locations for the rods. In a typical situation, the precise locations of the arrangement of absorbers to be identified are not necessarily known *a priori* and a much larger set of calibration states has to be employed. If an actual absorber is placed in between the grid positions for which the calibration states are known, are the resulting weights equally distributed among those two direct neighbors? Or do we require the weight of other basis states associated with rods being even farther away? The latter scenario would be similar to the leakage phenomenon [20] that occurs in numerical Fourier transformations if the actual frequency in a signal is not represented on a (discrete) frequency grid. In cases for which many single-rod calibration data are necessary to provide a sufficient spatial resolution, the required shadow function might be obtained by nonlinear extrapolations based on a smaller number of measured data. On the other hand, if the calibration data become linearly dependent of each other, a possible multiple-regression analysis might become unreliable as the inversion of a singular matrix would be required.

Our theoretical analysis has suggested that the technique becomes more accurate for systems that have large scattering coefficients. At the same time we observed that the corresponding shadow functions become more similar to each other and even blurred [21–23], which could jeopardize an unambiguous inversion. Furthermore, if the experimentally

unavoidable level of noise exceeds the difference between the shadow patterns of two neighboring rods, a unique assignment of the weights will no longer be possible. More systematic theoretical studies that include additive and also multiplicative noise need to be performed to examine the robustness of the technique.

The present experimental data used partially reflecting rods as absorbers. Theoretically we only examined absorbers as light modifying objects whose location was to be recovered. The quality of the inversion data suggests that the same technique might also work for nonabsorbing but highly scattering objects. Again, a similar theoretical analysis based on the consecutive application of various operators (as we discussed in Sec. II) could be employed in which the object would be described as a localized scatterer. In a recent work we have studied the invertibility of these transfer-matrix-like approaches to recover the position dependence of the scattering coefficient [24] and similar approaches could be examined.

The overall goal is to use the determined weights to deduce the position of the hidden objects. As we have seen, for absorbers whose illumination is partially blocked by other absorbers that are closer to the light source, the corresponding weights can be small and it might be difficult to distinguish these weights from those associated with no absorber. One could think of possible iterative schemes that can deduce the true presence of an absorber from the data. For instance, we have seen that those absorbers that are closest to the source are easiest to identify, as their weight factors are ideally equal to unity. In contrast to a rod that is not blocked by another absorber and should have an appreciable weight, the weight of a second (blocked) absorber cannot be expected to be that large. An algorithm can take these facts into account and modify correspondingly the threshold values (to determine the existence of a possible rod) for the weights.

As discussed above, the theoretical downstream model was purposely oversimplified to provide some qualitative features of the scheme and the scaling of the reliability with various parameters. For example, the precise functional form of the scattering kernel that we chose Gaussian can be modified to better represent a diffusive system.

In order to reduce the number of measurements of brightness patterns for given absorbers, the calibration data could be obtained from Monte Carlo simulations; however, in this case a better understanding of the scattering properties of the background medium would be required *a priori*.

We should finish this paper with a comment about the relationship of the nonlinear decomposition-based method discussed here and linear methods that were used in the mid-1990s in diffusive imaging [25,26] to reconstruct directly the spatially dependent part of the scattering and absorption coefficients $\delta\mu_s(r)$ and $\delta\mu_a(r)$. The early pioneering works used the diffusion approximation as the forward model and the Born approximation for the inverse problem. This approximation requires that the intensity associated entirely with the scattering of the heterogeneity be much smaller than the background light in the absence of the hidden object. As a result, the corresponding term in the integral form of the diffusion equation can be omitted and the scattered light becomes linear in the spatially dependent part of the scattering and absorption coefficients $\delta\mu_s(r)$ and $\delta\mu_a(r)$. Based on the measured light distribution relative to the background, a Fredholm integral equation of the first kind needs to be inverted. To obtain the required exact inversion, sometimes sophisticated iterative inversion techniques are necessary. A different approach—fluorescence tomography—is also based on the Born approximation and has recently been shown to lead to *in vivo* imaging of mice with remarkable resolution [27–30].

There are differences between the Born approximation and the nonlinear decomposition-based technique; e.g., the scaling of the practical limits of the schemes are different, and in fact, they are opposite to each other. While the Born-approximation method works best if the contrast between the object's optical scattering properties and that of the background medium is small, permitting a linear response, the nonlinear decomposition method requires a large contrast. The emphasis of the present work is to explore the region where absorbers block each other such that the resulting scattered light is no longer linear and the Born approximation fails. On the other hand, the method is presently based on prior knowledge of the images associated with single absorbers in the medium. This requirement could make this approach less practical for situations in which these *a priori* calibration measurements are difficult.

We will devote a future work [31] to discussing improvements of the scattering kernel for the downstream model, the sensitivity of the decomposition scheme to noise, the accuracy of predicting the location of absorbers that are located off the grid defined by the calibration states, and also an algorithm to improve the quantitative interpretation of the weights.

ACKNOWLEDGMENTS

This work has been supported by the NSF. We thank Professor P. Yu (U. Missouri, Columbia) for the loan of a special fiber, T. Blood for glass blowing, J. Dunham for detection table manufacturing, and Professor D. Cedeno, Professor B.K. Clark, Professor D. Marx, and Professor G.H. Rutherford for advice. We also acknowledge support from Research Corporation for Cottrell Science Awards and support from BLV.

[1] A. Ishimaru, *Wave Propagation and Scattering in Random Media* (Academic, New York, 1978), Vols. 1 and 2.
[2] S. Chandrasekhar, *Radiative Transfer* (Clarendon Press, Oxford, 1950).
[3] V. V. Tuchin, Laser Phys. **40**, 495 (1997).
[4] E. P. Zege, A. P. Ivanov, and I. L. Katsev, *Image Transfer though a Scattering Medium* (Springer-Verlag, Berlin, 1991).
[5] G. M. L. Gladwell, *Inverse Problems in Scattering* (Kluwer Academic, Dordrecht, 1993).
[6] O. Dorn, Inverse Probl. **14**, 1107 (1998).
[7] For a special issue on diffusive imaging, see Opt. Express **4** (8) (1999).
[8] *The Essential Physics of Medical Imaging*, 2nd ed., edited by J. T. Bushberg, J. A. Seibert, E. M. Leidholdt, Jr., and J. M. Boone (Lippincott Williams & Wilkins, Philadelphia, 2002).
[9] S. R. Arridge, Inverse Probl. **15**, R41 (1999).
[10] M. Born and E. Wolf, *Principles of Optics*, 7th ed. (Cambridge University Press, Cambridge, England, 1999).
[11] E. Hecht, *Optics* (Addison-Wesley, Reading, MA, 1987).
[12] B. E. A. Saleh and M. C. Teich, *Fundamentals of Photonics* (Wiley, New York, 1991).
[13] A. Refregier, Mon. Not. R. Astron. Soc. **338**, 35 (2003).
[14] J. Weissman, T. Hancewicz, and P. Kaplan, Opt. Express **12**, 5760 (2004).
[15] I. L. Katsev, E. P. Zege, and A. S. Prikhach, Appl. Opt. **38**, 6849 (1999).
[16] See, e.g., R.C. Aster, B. Borchers, and C.H. Thurber, *Parameter Estimation and Inverse Problems* (Elsevier, Amsterdam, 2005).
[17] S. Campbell, S. Menon, Q. Su, G. H. Rutherford, and R. Grobe, Laser Phys. **17**, 117 (2007).
[18] S. D. Campbell, A. K. O'Connell, S. Menon, Q. Su, and R. Grobe, Phys. Rev. E **74**, 061909 (2006).
[19] S. Campbell, A. D. O'Connell, G. H. Rutherford, and R. Grobe, Opt. Lett. **32**, 560 (2007).
[20] P. L. DeVries, *Computational Physics* (Wiley, New York, 1994).
[21] Z. Liu, Y. Yu, K. Zhang, and H. Huang, Opt. Eng. **40**(6), 1125 (2001).
[22] A. Rav-Acha and S. Peleg, Pattern Recog. Lett. **26**, 311 (2005).
[23] P. C. Hansen, J. G. Nagy, and D. P. O'Leary, *Deblurring Images: Matrices, Spectra and Filtering* (Siam, Philadelphia, 2006).
[24] K. D. Lamb, S. Menon, Q. Su, and R. Grobe, Phys. Rev. E **74**, 061903 (2006).
[25] For more detailed accounts of the Born approximation, see D.A. Boas, Ph.D. thesis, University of Pennsylvania, 1996 (unpublished); M.A. O'Leary, Ph.D. thesis, University of Pennsylvania, 1996 (unpublished).
[26] M. A. O'Leary, D. A. Boas, B. Chance, and A. G. Yodh, Opt. Lett. **21**, 158 (1996).
[27] V. Ntziachristos and R. Weissleder, Opt. Lett. **26**, 893 (2001).
[28] E. E. Graves, J. Ripoll, R. Weissleder, and V. Ntziachristos, Med. Phys. **30**, 901 (2003).
[29] For a recent review on fluorescence diffuse tomography, see A. Corlu, R. Choe, T. Durduran, M.A. Rosen, M. Schweiger, S.R. Arridge, M.D. Schnall, and A.G. Yodh, Opt. Express **15**, 6696 (2007) and many references therein.
[30] R. Weissleder and V. Ntziachristos, Nature (London) **9**, 123 (2003).
[31] S.D. Campbell, S. D. Grobe, I. L. Goodin, Q. Su and R. Grobe (unpublished).